Atomically Precise Copper Alloy Nanoclusters for the Electrochemical Reduction of CO to Value-Added Chemicals

Shomokh Hamad Alharbi
shomokhhrb@gmail.com

Mentor: Dr. Bodiuzzaman Mohammad
bodiuzzaman.mohammad@kaust.edu.sa

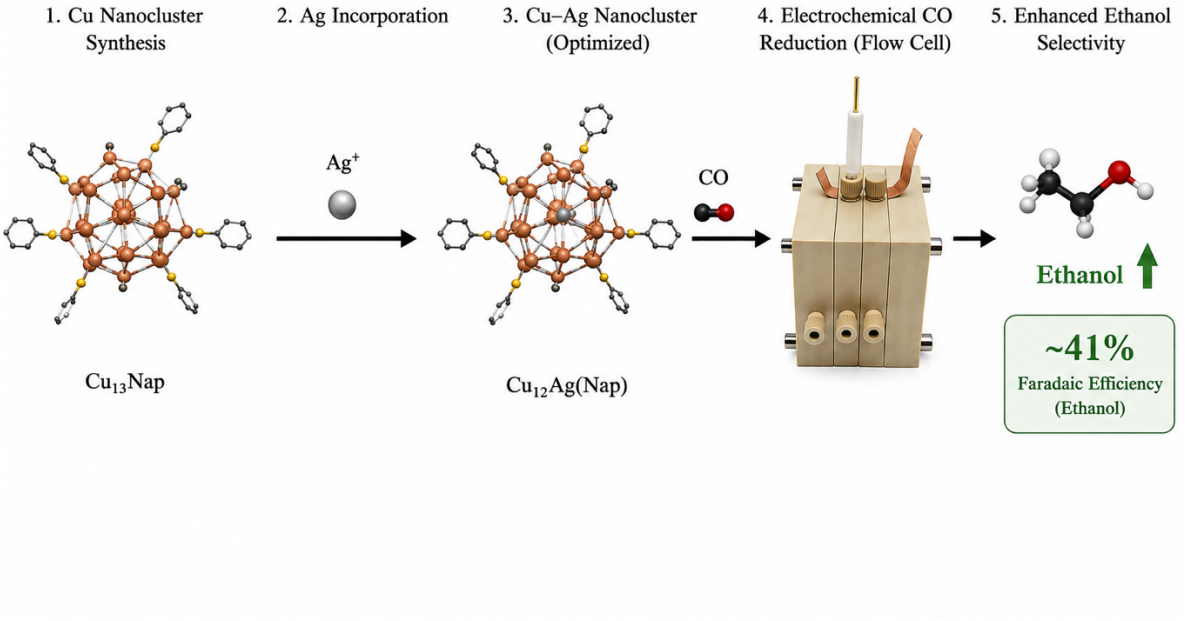
PI: Prof. Osman M. Bakr
Functional Nanomaterials Lab (FuNL)
Physical Science and Engineering (PSE) Division

KAUST Academy Energy Transition Internship Program Report

King Abdullah University of Science and Technology (KAUST)
Thuwal, Saudi Arabia
August 24, 2026

Abstract

Atomically precise copper-based nanoclusters provide a promising platform for controlling product selectivity in the electrochemical reduction of carbon monoxide (CO). In this work, Cu and Cu–Ag nanoclusters with different ligand environments were synthesized and characterized by electrospray ionization mass spectrometry (ESI-MS), X-ray photoelectron spectroscopy (XPS), UV–Vis spectroscopy, and single-crystal X-ray diffraction, providing evidence for the formation of Ag-containing Cu nanocluster species. Selected nanoclusters were evaluated for electrochemical CO reduction in a flow-cell configuration, with liquid products quantified by ^{1}H NMR spectroscopy. Cu-only nanoclusters predominantly produced acetate, while the Ag-incorporated $Cu_{12}Ag$(Nap) nanocluster exhibited significantly enhanced selectivity toward ethanol production. The optimized $Cu_{12}Ag$(Nap) system reached approximately 41% Faradaic efficiency for ethanol, representing a substantial enhancement compared with the Cu-only systems. These results demonstrate that atomic-level compositional control through Ag incorporation can be an effective strategy for tuning CO-reduction pathways toward value-added products.



Contents

1 Introduction 4
2 Related Work 4
3 Methodology 5
3.1 Preparation of Cu Precursor 5
3.2 Synthesis of Cu_{13}Nap Nanoclusters 5
3.3 Ag Incorporation and Synthetic Optimization 5
3.4 Selected Cu-Ag Nanocluster Synthesis 6
3.5 Synthesis of PFBT-Protected Cu3 and Cu3Ag Nanoclusters 6
3.6 Crystallization 6
3.7 Characterization 6
3.8 Electrochemical CO Reduction 7
4 Results and Discussion 7
4.1 Reference Cu Nanocluster Characterization 7
4.2 Cu_3Ag Nanocluster Characterization 8
4.3 ESI-MS Spectrum of the Ag-incorporated Cu Nanoclusters 9
4.4 UV-Vis Characterization of Cu_{13}Nap and Cu_{12}AgNap 10
4.5 Crystallization Behavior 11
4.6 Electrochemical CO Reduction Performance 11
5 Limitations and Future Work 12
6 Conclusion 13
7 Acknowledgment 13
8 References 13

1 Introduction

The continued reliance on fossil-derived carbon to produce fuels and chemical feedstocks has increased the need for more sustainable approaches to carbon utilization. Electrochemical carbon conversion offers a promising route that uses electrical energy to convert simple carbon-containing molecules, such as CO_2 and CO, into value-added fuels and chemicals under relatively mild reaction conditions. Of particular interest is the formation of multicarbon (C_2+) products, although selectively promoting C–C bond formation and directing the reaction toward a desired product remain major challenges [1].
Carbon monoxide is an important intermediate in the electrochemical conversion of CO_2 and can undergo further electrochemical reduction to form C_2+ products such as ethylene, ethanol, and acetate. Among these products, ethanol is particularly attractive as a liquid fuel and chemical feedstock with practical advantages in storage and transportation. Its formation involves C–C coupling followed by multiple proton- and electron-transfer steps within a complex reaction network, making selective ethanol production difficult [2]. Copper (Cu) is particularly important for CO reduction (CORR) because of its ability to promote C–C coupling and generate multicarbon products. This behavior is closely related to its interaction with adsorbed CO (*CO), which enables further coupling and reduction of carbon-containing intermediates. However, the ability of Cu to stabilize multiple intermediates also allows competing reaction pathways to occur, limiting its selectivity toward individual products [3].

The catalytic behavior of Cu is also strongly influenced by its atomic and surface structure. Conventional Cu nanoparticles contain different surface environments, including terraces, edges, defects, and differently coordinated Cu atoms, which can interact differently with reaction intermediates. In addition, structural reconstruction may occur under electrochemical conditions, further complicating the identification of active sites and the relationship between catalyst structure and product selectivity. Atomically precise Cu nanoclusters provide a useful platform for addressing this limitation because they contain a well-defined number of metal atoms and possess discrete compositions. Their atomic-level definition allows the effects of changes in composition and structure on catalytic behavior to be investigated in a more systematic way [4].

Further control can be achieved by incorporating a second metal into the Cu nanocluster. Alloying can modify the electronic structure and local coordination environment of Cu sites, potentially altering the adsorption and stabilization of key intermediates and, consequently, the distribution of CORR products. However, these effects depend strongly on the identity and atomic arrangement of the incorporated metal, and their relationship with catalytic selectivity is not yet fully understood [5]. In this work, we synthesized atomically precise Cu-based clusters, including Ag-doped Cu_{13} nanoclusters and the $Cu_3(PFBT)_4$ and $Cu_3Ag(PFBT)_5$ systems, with PFBT as pentafluorobenzenethiol. The Ag-doped Cu_{13} nanoclusters were protected by naphthalene thiol and PPh_3. These NCs were characterized by ESI MS, XPS, and UV-vis. Remarkably, a one-atom change led to a dramatic shift in product distribution, from acetate-dominant to ethanol-dominant.

2 Related Work

Recent work by Bodiuzzaman et al. has established ligand-modified copper nanoclusters (NCs) as a platform for probing structure selectivity relationships in CORR. High-nuclearity Cu NCs stabilized by thiol-based ligands were engineered toward CO-to-acetate conversion by tuning local hydrophobicity and the balance between ligand coverage and active-site exposure. The resulting Cu_{13}Nap catalyst achieved an acetate Faradaic efficiency of 69%. Computational and

operando spectroscopic analyses further revealed that asymmetric Cu–Cu coordination environments, rather than nuclearity alone, govern CO binding strength and influence the reaction pathway following C–C coupling [1].

Complementary studies have examined how ligand modification and local coordination influence pathway selection in smaller Cu nanoclusters. Systematic variation of the ligand electronic environment showed that changes in electron-donating and electron-withdrawing character can alter the hydrogenation of surface intermediates and consequently shift product selectivity [6]. In addition, introducing mixed Cu–S, N coordination environments demonstrated that changes in the local symmetry of Cu sites can substantially modify carbon-reduction pathways and promote the formation of multicarbon products [7].

Together, these studies demonstrate that both the local coordination structure and ligand environment can strongly influence intermediate binding and pathway selection in Cu nanoclusters. These findings provide a basis for extending atomic-level control beyond ligand and coordination engineering toward compositional alloying, where the incorporation of a second metal offers an additional approach for tuning CORR product selectivity.

3 Methodology

3.1 Preparation of Cu Precursor

The Cu(I) precursor was prepared by reacting Cu_2O (3 g) with acetonitrile (ACN, 25 mL), followed by the addition of HBF_4 (15 mL). The mixture was heated at 70 °C for 1 h under ambient conditions, after which the resulting product was collected by filtration, washed with ACN, and dried under vacuum for 1 h. The obtained Cu(I) complex was subsequently used as the copper precursor for nanocluster synthesis.

3.2 Synthesis of Cu_{13}Nap Nanoclusters

Cu_{13}Nap nanoclusters were synthesized following a previously reported procedure with minor modifications [8]. The Cu precursor (100 mg) was dissolved in ACN (4 mL) and stirred for 5 min. Nap (30 µL) was then added, followed by another 5 min of stirring. PPh_3 (35 mg), dissolved in $CHCl_3$ (1 mL) was then added. After 15 min, freshly prepared $NaBH_4$ (70 mg in 5 mL MeOH) was introduced as the reducing agent, and the reaction mixture was stirred for 3 h. This procedure served as the reference synthesis for subsequent Ag incorporation and optimization experiments.

3.3 Ag Incorporation and Synthetic Optimization

Ag incorporation into the Cu-based nanoclusters was initially investigated by modifying the established Cu_{13}Nap synthesis. Different Ag loadings were evaluated, followed by systematic modification of the ligand, solvent environment, Ag precursor, reduction conditions, crystallization conditions, and order of precursor addition.
These experiments were conducted as part of a systematic optimization of the Cu–Ag nanocluster synthesis. The main experimental variations are summarized in Table 1.

Table 1. Summary of the main optimization experiments for Cu-Ag nanocluster synthesis.

Optimization parameter	Conditions investigated
Ag loading	CF_3COOAg: 1-7 mg, subsequently increased up to 40mg
Ligand modification	Nap, TFBT, and DCBT
Metal exchange	Post-synthetic introduction of Ag into preformed Cu NCs
Solvent	$CHCl_3$/DCM, and toluene
Ag precursor	CF_3COOAg and $AgNO_3$
Reduction	Conventional and slow reduction
Pre-coordination	Modified metal/ligand addition sequence

3.4 Selected Cu-Ag Nanocluster Synthesis

Following the optimization experiments, the selected Cu–Ag nanocluster synthesis was carried out using 45 mg of the Cu precursor dissolved in 4 mL of ACN. The mixture was stirred for 5 min, followed by the addition of CF_3COOAg (40 mg). After another 5 min, Nap (30 µL) was added and the mixture was stirred for an additional 5 min. PPh_3 (35 mg), dissolved in 1 mL of DCM, was then introduced. After 30 min of stirring, freshly prepared $NaBH_4$ (70 mg in 5 mL of MeOH) was added as the reducing agent, and the reaction mixture was stirred for 3 h.

3.5 Synthesis of PFBT-Protected Cu3 and Cu3Ag Nanoclusters

PFBT-protected Cu_3 nanoclusters were prepared by dispersing $Cu(NO_3)_2 \cdot 3H_2O$ (12 mg) in ethanol (5 mL), followed by sonication. PFBT (20 µL) was then added, and the mixture was further sonicated.

For the Cu_3Ag system, $Cu(NO_3)_2 \cdot 3H_2O$ (12 mg) was dispersed in ethanol (5 mL) and sonicated, followed by the addition of PFBT (20 µL). An Ag precursor solution was separately prepared by dissolving CF_3COOAg (15 mg) in ACN (1.5 mL), and 100 µL of this solution was added to the reaction mixture. The resulting mixture was further sonicated before subsequent processing.

3.6 Crystallization

Crystallization was attempted for most of the synthesized Cu- and Cu–Ag-based nanocluster samples using various solvent/antisolvent combinations, including hexane, diethyl ether, and methanol as antisolvents. Despite these efforts, single crystals suitable for X-ray diffraction were obtained for only one sample: the Cu–Ag nanocluster synthesized using the Cu(I) precursor (100 mg) in ACN, 2,4-dichlorobenzenethiol (30 µL), $AgCF_3COO$ (10 mg), PPh_3 (35 mg) dissolved in DCM (1 mL), and $NaBH_4$ (70 mg in 5 mL MeOH) as the reducing agent. Crystals were grown by dissolving the crude product in DCM followed by slow diffusion of hexane as the antisolvent, with the solution stored at 4 °C for one month. The resulting single crystals were used to confirm the nanocluster structure by single-crystal X-ray diffraction.

3.7 Characterization

The synthesized nanoclusters were characterized using UV–Vis spectroscopy, electrospray ionization mass spectrometry (ESI-MS), X-ray photoelectron spectroscopy (XPS), and single-crystal X-ray diffraction (SC-XRD). UV–Vis spectroscopy was used to monitor the optical characteristics of the synthesized samples over a wavelength range of 200–800 nm. ESI-MS

was performed in positive and negative ion mode to evaluate cluster composition and confirm Ag incorporation. XPS survey scans (0–1200 eV binding energy) were used to investigate the elemental composition and chemical states of the metal species, confirming the presence of Cu, Ag, and ligand-derived elements (C, F, P). For the single sample that yielded crystals suitable for structural analysis, SC-XRD was performed to determine the nanocluster's molecular structure.

3.8 Electrochemical CO Reduction

Electrochemical CO reduction was performed in a flow-cell configuration using the synthesized Cu–Ag nanoclusters as the electrocatalyst. The catalyst was spray-coated onto carbon paper and used as the working (cathodic) electrode, with IrO_2 serving as the anode. An Ag/AgCl reference electrode was used in a three-electrode configuration, and a Nafion membrane separated the cathodic and anodic compartments. A 1 M KOH solution was used as the electrolyte in both the cathodic and anodic compartments. Electrolysis was performed under continuous CO flow at stepwise increasing current densities (e.g., 50 and 100 mA/cm^2), with each step maintained for 30 min. Following electrolysis, the liquid products were collected and analyzed by ^{1}H NMR spectroscopy using D_2O for product identification and quantification.

4 Results and Discussion

4.1 Reference Cu Nanocluster Characterization

The Cu nanocluster system was first characterized by (ESI-MS) to establish a compositional reference before Ag incorporation. The experimental mass spectrum showed a dominant signal at m/z = 987.58, assigned to $[Cu_3(PFBT)_4]^-$. The experimental isotopic pattern closely matched the simulated pattern for this composition, confirming the Cu_3 cluster nuclearity and providing the baseline structure against which subsequent Ag-doped systems were compared (Figure 1). XPS analysis was also performed to further characterize the $Cu_3(PFBT)_4$ nanocluster (Figure 2). The survey spectrum confirmed the presence of Cu and ligand-derived elements, while the Cu 2p and Cu LMM Auger spectra showed that the chemical state of Cu is +1.

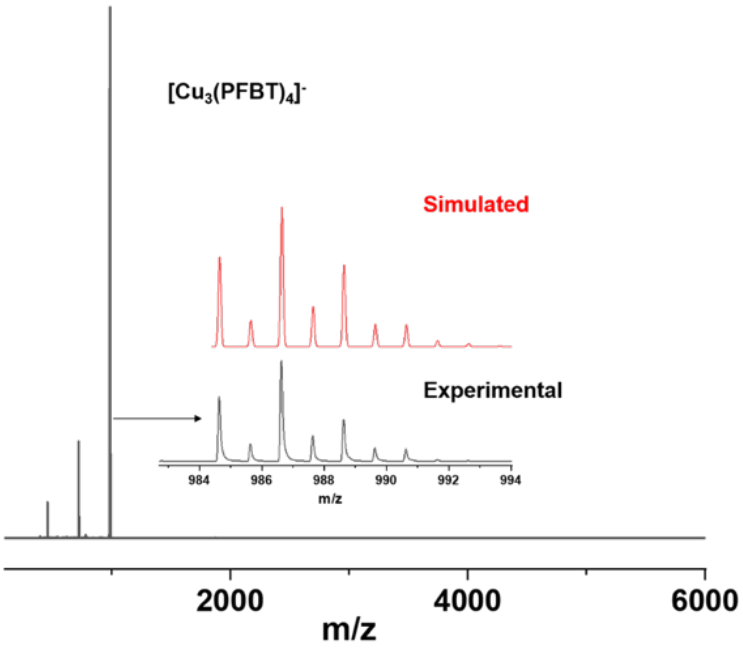


Figure 1. ESI-MS spectrum of the $Cu_3(PFBT)_4$. nanocluster, including comparison of the experimental and simulated isotopic patterns.

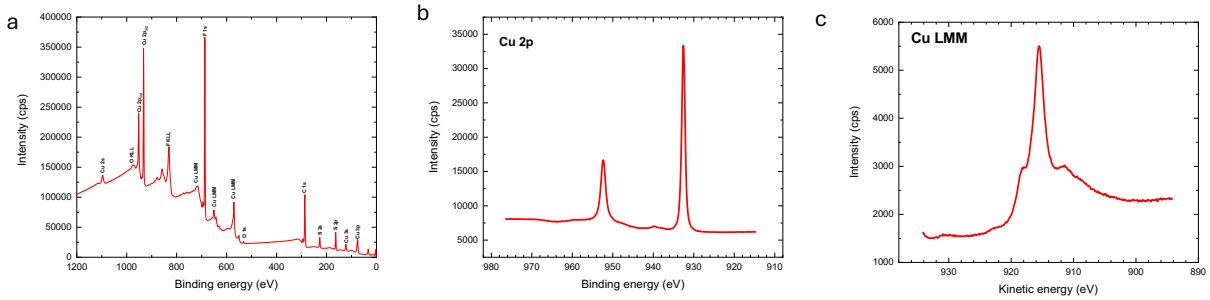


Figure 2. XPS characterization of $Cu_3(PFBT)_4$. (a) XPS survey spectrum; (b) Cu 2p core-level spectrum; and (c) Cu LMM Auger spectrum.

.

4.2 Cu_3Ag Nanocluster Characterization

Building on this reference system, Ag incorporation was first investigated through the synthesis of the PFBT-protected Cu_3Ag nanocluster. ESI-MS showed a dominant signal at m/z = 1294.55, assigned to $[Cu_3Ag(PFBT)_5]^-$. Notably, the experimental peak was shifted relative to the $Cu_3(PFBT)_4$ reference by a mass difference corresponding to a single Ag atom substitution, providing direct evidence that Ag had been incorporated into the cluster core rather than merely associated with the surface ligand shell. The close match between the experimental and simulated isotopic distributions further supported this assignment (Figure 3). XPS analysis further supported the presence of both Cu and Ag in the $Cu_3Ag(PFBT)_5$ nanocluster (Figure 4). The survey spectrum showed signals corresponding to both metals, while the Cu 2p and Cu LMM Auger spectra, together with the Ag 3d and Ag MNN Auger spectra, provided further information on their chemical states, consistent with the successful incorporation of Ag observed by ESI-MS.

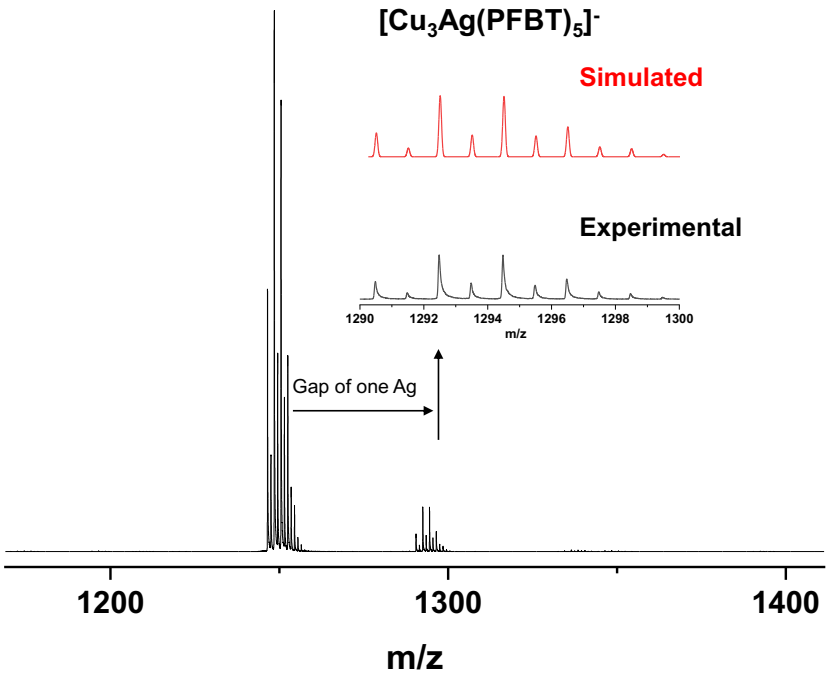


Figure 3. ESI-MS spectrum of the $Cu_3Ag(PFBT)_5$. nanocluster showing the experimental and simulated isotopic distributions

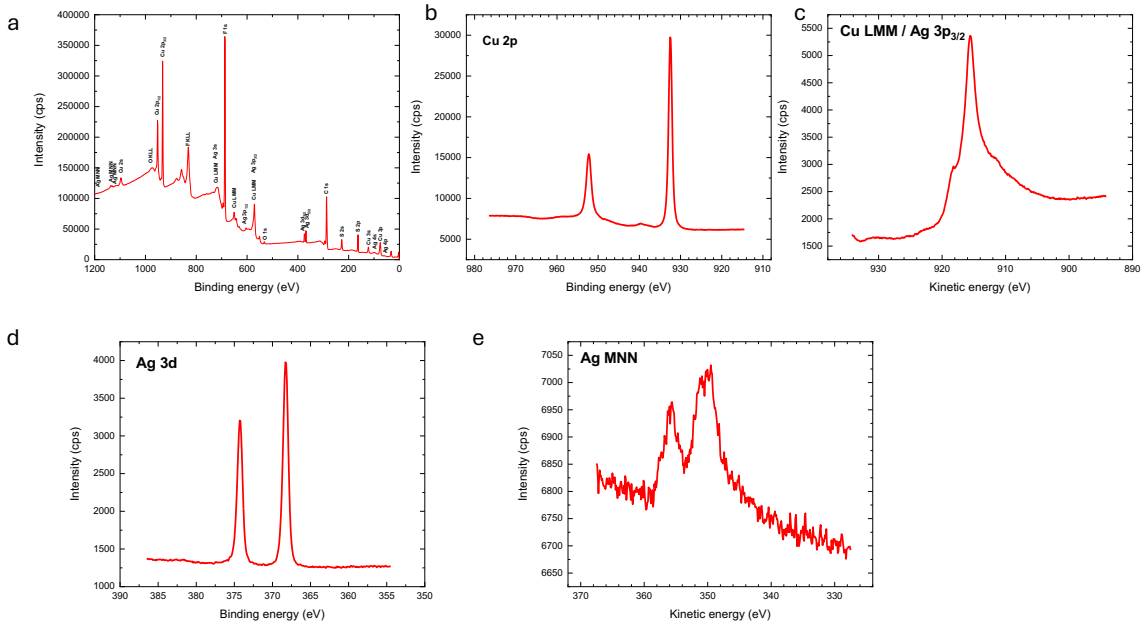


Figure 4. XPS characterization of $Cu_3Ag(PFBT)_5$. (a) XPS survey spectrum. (b,c) Cu 2p core-level and Cu LMM Auger spectra, respectively. (d,e) Ag 3d core-level and Ag MNN Auger spectra, respectively.

4.3 ESI-MS Spectrum of the Ag-incorporated Cu Nanoclusters

To evaluate whether this Ag-incorporation behavior extended to a structurally distinct ligand system, ESI-MS was used to investigate Ag incorporation into Nap-protected Cu nanoclusters. The spectrum showed a signal at m/z = 3518.896, assigned to $[Cu_{12}Ag(Nap)_3(PPh3)_7]$ with an attached $[CuPPh_3]^+$. This type of gas-phase adduct formation is commonly observed in ESI-MS analysis of ligand-protected nanoclusters and does not indicate a distinct cluster species. The detection of the Ag-containing

$[Cu_{12}Ag(Nap)_3(PPh_3)_7]^+$ species confirms successful Ag incorporation into the Nap-protected Cu nanocluster system (Figure 5).

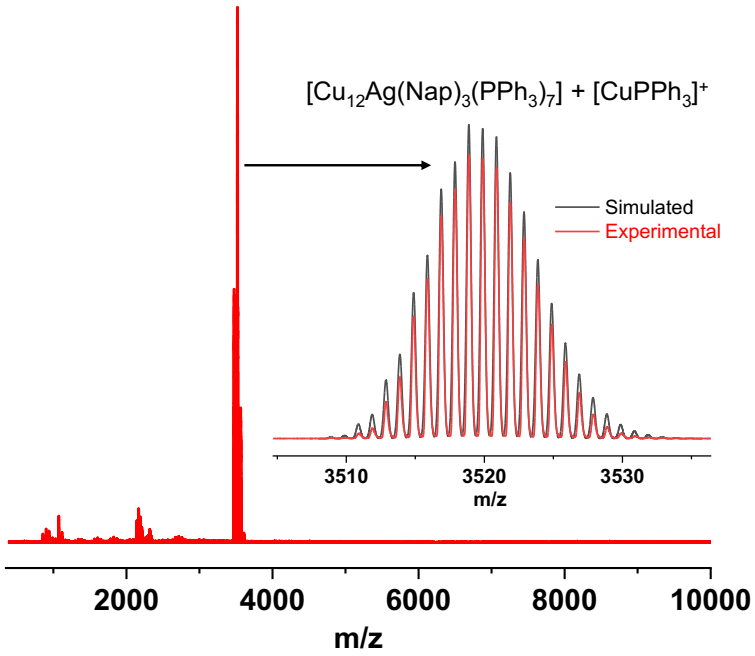


Figure 5.ESI-MS spectrum of the Ag-incorporated Cu nanocluster showing the assigned Ag-containing cluster species.

4.4 UV-Vis Characterization of Cu_{13}Nap and Cu_{12}AgNap

UV–Vis absorption spectroscopy was used to compare the optical properties of the reference Cu_{13}Nap nanocluster and the Ag-incorporated Cu_{12}AgNap system (Figure 6). Both nanoclusters exhibited a decrease in absorbance with increasing wavelength across the 350–800 nm range. Notably, the Cu_{12}AgNap spectrum showed a broader absorption profile relative to Cu_{13}Nap, with absorbance decaying more gradually across the measured wavelength range, suggesting that Ag incorporation may influence the electronic structure of the nanocluster. Further spectroscopic and computational analysis would be needed to assign these optical features to specific electronic transitions.

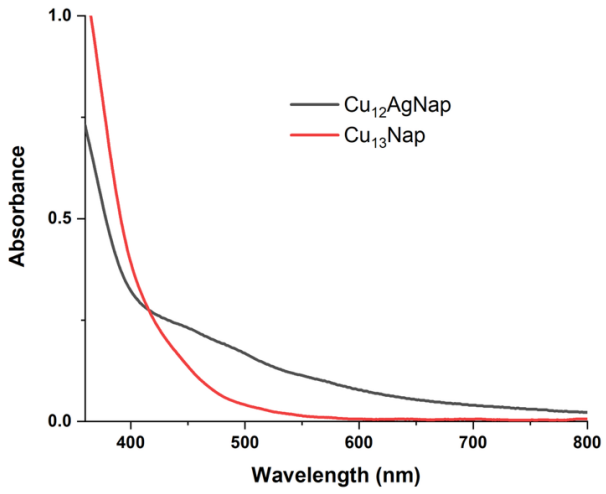


Figure 6. UV–Vis absorption spectra of Cu_{13}Nap and Cu_{12}AgNap nanoclusters.

4.5 Crystallization Behavior

Crystallization was investigated for several synthesized Cu–Ag nanocluster samples using different solvent/antisolvent combinations. Initial attempts using hexane, diethyl ether, and methanol as antisolvents did not yield any crystalline material. Among the ligand systems investigated, the use of 2,4-dichlorobenzenethiol (DCBT) as the protecting ligand, followed by slow diffusion of hexane into a DCM solution of the crude product over one month at 4 °C, resulted in the formation of single crystals. However, ESI-MS analysis of this sample showed only a weak Ag-containing cluster signal, indicating that favorable crystallization behavior did not necessarily correspond to efficient Ag incorporation into the Cu nanocluster core. Structural analysis of these crystals by single-crystal X-ray diffraction is currently in progress and may help clarify whether Ag is present at low occupancy within the crystallized phase or largely absent from this structure. Crystallization efforts of other samples like $Cu_{12}Ag$ NCs are underway.

4.6 Electrochemical CO Reduction Performance

Selected Cu- and Cu–Ag-based atomically precise nanoclusters were evaluated as electrocatalysts for the electrochemical reduction of carbon monoxide (CO) in a flow-cell configuration. The flow-cell architecture was employed to provide an efficient supply of CO to the catalyst layer and to enable evaluation under conditions relevant to practical gas-fed electrochemical CO conversion. Emphasis was placed on the formation of C_2 oxygenates, especially ethanol, given the ability of Cu-based catalysts to facilitate C–C coupling during CO reduction.

The liquid-phase products generated during electrolysis were collected and quantitatively analyzed by **^{1}H NMR spectroscopy**, with specific attention to ethanol and acetate. Faradaic efficiencies (FEs) were calculated based on the quantity of each detected product relative to the total charge passed during electrolysis. The product distributions revealed a strong dependence of catalytic behavior on both the nanocluster composition and the surface ligand **environment**, highlighting the importance of precise structural and electronic control at the nanocluster level.

The Cu_{13}Nap and Cu_{13}DCBT nanoclusters exhibited predominantly **acetate formation**, while ethanol was produced only as a minor product, with Faradaic efficiencies of approximately **8–9% (Figure 7)**. This product distribution indicates that these Cu-only nanoclusters favor pathways leading toward acetate rather than efficient formation and stabilization of ethanol. The difference between the two ligand environments further suggests that the surface coordination environment surrounding the Cu framework can influence the reaction pathway and the relative rates of competing C_{2+} product-forming processes.

In contrast, incorporation of Ag into the Cu nanocluster framework resulted in a pronounced change in product selectivity. The **Cu_{12}Ag(Nap)** nanocluster exhibited the highest ethanol Faradaic efficiency among the nanoclusters investigated, reaching approximately **41% FE for ethanol (Figure 7)**. This represents a substantial enhancement in ethanol selectivity compared with the Cu_{13}Nap and Cu_{13}DCBT systems and demonstrates that controlled Ag incorporation can significantly modify the catalytic behavior of Cu-based nanoclusters.

The enhanced ethanol production observed for $Cu_{12}Ag$(Nap) may arise from changes in the electronic structure and local coordination environment introduced by Ag incorporation. In addition to electronic effects, Ag doping can alter the distribution and accessibility of catalytically active Cu sites, potentially modifying CO adsorption, C–C coupling, and the subsequent hydrogenation steps required for ethanol formation. The ligand environment may further regulate the interfacial properties of the nanocluster, including reactant accessibility and the local reaction environment. These factors provide potential explanations for the substantial shift from acetate-dominated selectivity in the Cu-only nanoclusters toward enhanced ethanol formation in the Cu–Ag system [9].

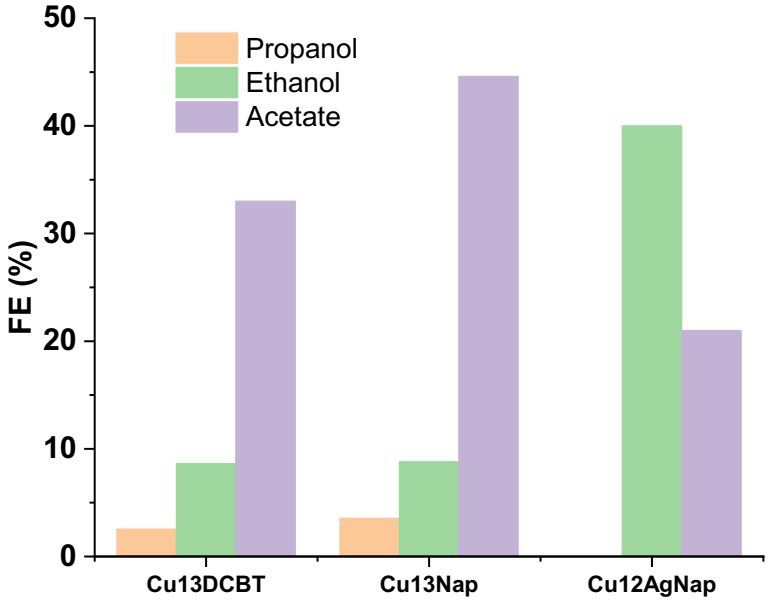


Figure 7. Faradaic Efficiencies of Various Catalysts for CORR at a Current Density of 50 mA cm⁻².

5 Limitations and Future Work

Several aspects of the present study warrant further investigation to clarify the relationship among Ag incorporation, nanocluster composition, and catalytic selectivity. Gas-phase products were not quantified in this work; future studies could incorporate gas chromatography (GC) analysis to establish a more complete Faradaic efficiency balance across the reaction products. Although ESI-MS provided evidence for the formation of Ag-containing nanocluster species, the precise location and coordination environment of Ag within the Cu framework remain unresolved. Further structural characterization would help clarify the relationship among Ag incorporation, nanocluster structure, and catalytic selectivity. The observed correlation between enhanced Ag incorporation and increased ethanol Faradaic efficiency in the optimized $Cu_{12}Ag$(Nap) system is currently based on a single sample. Investigating additional Cu–Ag nanoclusters with different Ag loadings would help determine whether this represents a consistent structure–selectivity relationship. Finally, several synthetic parameters, including ligand identity, Ag precursor, solvent environment, and reduction conditions, were explored during optimization. Future studies should employ a more systematic approach to identify conditions that promote Ag incorporation while improving selectivity toward C_{2+} products.

6 Conclusion

In this work, atomically precise Cu–Ag nanoclusters were investigated for electrochemical CO reduction, with emphasis on the influence of Ag incorporation on catalytic selectivity. ESI-MS provided evidence for Ag-containing nanoclusters in both PFBT- and Nap-protected systems. Overall, these results demonstrate that **atomically precise control over both metal composition and ligand coordination provides an effective strategy for tuning CO-reduction pathways**. The comparison between Cu-only and Cu–Ag nanoclusters establishes a clear correlation between nanocluster composition and C_{2+} product selectivity, with Ag incorporation leading to a significant enhancement in ethanol formation. The $Cu_{12}Ag$ (Nap) nanocluster therefore represents a promising platform for further investigation of selective electrochemical CO-to-ethanol conversion. Future studies should focus on correlating the atomically resolved structure, Ag distribution, ligand coordination, and electronic properties of these nanoclusters with their catalytic performance to identify the structural features responsible for enhanced C–C coupling and ethanol selectivity.

7 Acknowledgment

I want to express my sincere gratitude to Prof. Osman M. Bakr for the opportunity to conduct this research in his group, and to Dr. Bodiuzzaman for his guidance and supervision throughout the project. I am also thankful to Renqian Zhou and Mohammed Alotaibi for their valuable assistance and support during the research.

On an institutional level, I extend my appreciation to King Abdullah University of Science and Technology (KAUST) and KAUST Academy for hosting this program and providing access to world-class facilities. Finally, I gratefully acknowledge King Abdullah City for Atomic and Renewable Energy (K.A.CARE) and the Center of Excellence for Renewable Energy and Storage Technologies (CREST) for their support throughout this research internship.

8 References

[1] M. Bodiuzzaman *et al.*, "High-Nuclearity Copper Molecular Catalysts for Electrocatalytic CO-to-Acetate Conversion," *J. Am. Chem. Soc.*, vol. 147, no. 35, pp. 31713–31721, Sep. 2025, doi: 10.1021/jacs.5c08144.

[2] C. Zhan *et al.*, "Key intermediates and Cu active sites for CO2 electroreduction to ethylene and ethanol," *Nat. Energy*, vol. 9, no. 12, pp. 1485–1496, Sep. 2024, doi: 10.1038/s41560-024-01633-4.

[3] C. W. Li, J. Ciston, and M. W. Kanan, "Electroreduction of carbon monoxide to liquid fuel on oxide-derived nanocrystalline copper," *Nature*, vol. 508, no. 7497, pp. 504–507, Apr. 2014, doi: 10.1038/nature13249.

[4] Q. Wu *et al.*, "Atomically Precise Copper Nanoclusters for Highly Efficient Electroreduction of CO_2 towards Hydrocarbons via Breaking the Coordination Symmetry of Cu Site," *Angew. Chem. Int. Ed.*, vol. 62, no. 36, p. e202306822, Sep. 2023, doi: 10.1002/anie.202306822.

[5] Y.-X. Wang, J. Li, F.-Q. Zhang, Z. Qi, F. Zhang, and X.-M. Zhang, "Investigation on Reactivity and Selectivity of Electrocatalytic CO_2 Reduction in Photochemically Synthesized Ag_{19} and Alloyed Ag_{19} Cu_2 and Ag_{12} Cu_7 Nanoclusters," *ACS Cent. Sci.*, vol. 11, no. 8, pp. 1428–1437, Aug. 2025, doi: 10.1021/acscentsci.5c00784.

[6] R. Zhou *et al.*, "Stepwise Ligand Tuning of Copper Clusters for CO2 Electroreduction Pathway Control," *ACS Mater. Lett.*, vol. 8, no. 8, pp. 2210–2219, Aug. 2026, doi: 10.1021/acsmaterialslett.6c00341.

[7] Q. Wu *et al.*, "Atomically Precise Copper Nanoclusters for Highly Efficient Electroreduction of CO_2 towards Hydrocarbons via Breaking the Coordination Symmetry of Cu Site," *Angew. Chem. Int. Ed.*, vol. 62, no. 36, p. e202306822, Sep. 2023, doi: 10.1002/anie.202306822.

[8] M. Bodiuzzaman *et al.*, "Modulating Decarboxylative Oxidation Photocatalysis by Ligand Engineering of Atomically Precise Copper Nanoclusters," *J. Am. Chem. Soc.*, vol. 146, no. 39, pp. 26994–27005, Oct. 2024, doi: 10.1021/jacs.4c08688.

[9] P. Iyengar, M. J. Kolb, J. R. Pankhurst, F. Calle-Vallejo, and R. Buonsanti, "Elucidating the Facet-Dependent Selectivity for CO_2 Electroreduction to Ethanol of Cu–Ag Tandem Catalysts," *ACS Catal.*, vol. 11, no. 8, pp. 4456–4463, Apr. 2021, doi: 10.1021/acscatal.1c00420.